iScience

CellPress
OPEN ACCESS

Article

Developmental correspondence of juvenile stages across the locust, harlequin ladybird, and diamondback moth

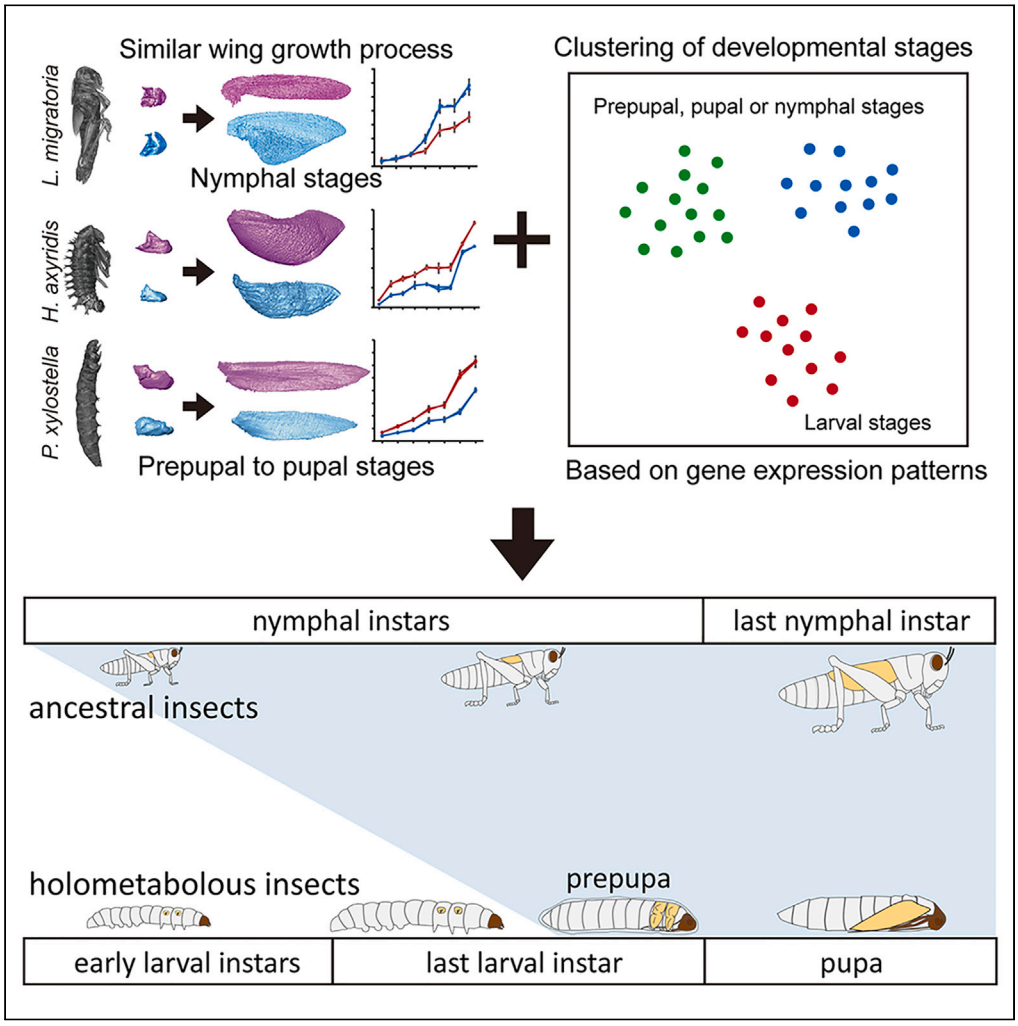

Hang Zhou, Runguo Shu, Chaowei Zhang, ..., Xi Chen, Yang Mei, Fei Li

zhouhang716@zju.edu.cn (H.Z.)
lifei18@zju.edu.cn (F.L.)

Highlights

Holometabolous prepupae and pupae exhibit a similar wing growth process to nymphs

Prepupae and pupae resembling nymphs with similar gene expression patterns

Gene expression during juvenile stages shows evolution toward increased time-specificity

Metamorphosis-biased genes retain more nucleotide substitutions

Zhou et al., iScience 27, 110898
October 18, 2024
https://doi.org/10.1016/j.isci.2024.110898

iScience

CellPress
OPEN ACCESS

Article

Developmental correspondence of juvenile stages across the locust, harlequin ladybird, and diamondback moth

Hang Zhou,[1,3,*] Runguo Shu,[1,3] Chaowei Zhang,[1] Yiqi Xiao,[1] Dong Jing,[1] Jiejing Tang,[1] Zixiong Cao,[2] Xi Chen,[1] Yang Mei,[1] and Fei Li[1,4,*]

SUMMARY

Insect metamorphosis is a captivating aspect of animal research. To address the controversy regarding the developmental correspondence between hemimetabolous and holometabolous insects, we utilized non-destructive micro-computed tomography (CT) imaging and RNA-seq to examine wing growth and transcriptome profiles across juvenile stages in the *Locusta migratoria*, *Harmonia axyridis*, and *Plutella xylostella*, with distinct metamorphic strategies. Micro-CT revealed that over 88% of wing volume increase in ladybirds and moths occurs during the prepupal-pupal transition, similar to locust nymphs. Developmental transcriptome clustering demonstrated that gene expression patterns more closely resembled those between ladybird/moth prepupae/pupae and locust nymphs, whereas holometabolous larvae exhibited distinct profiles. Notably, gene expression specificity increased across juvenile stages with more recent species divergence. Genes highly expressed around the prepupal/pupal stages accumulated higher evolutionary rates. These integrated findings unveil commonalities in juvenile stage development among the locust, ladybird, and moth, providing insights into the evolution of metamorphosis within neopteran insects.

INTRODUCTION

Insect metamorphosis is a captivating phenomenon in animal research. Neopteran insects can be classified into two main types of metamorphosis: hemimetabolism (incomplete metamorphosis) and holometabolism (complete metamorphosis). Holometabolous insects undergo significant morphological changes between their larval and adult stages, including the emergence of adult organs such as wings during the pupal stages.[1–3] These distinct developmental stages offer advantages in resource acquisition, facilitating rapid diversification and radiation within the holometabola.[4–6] The prevalence of holometabolous metamorphosis among extant insects, encompassing over 80% of described species, attests to its evolutionary success and ecological dominance within the Insecta.[7]

Phylogenetic analysis indicates that holometabolous insects evolved from their hemimetabolous ancestors.[8,9] Nevertheless, the origin and precise homology of the pupa have long been subjects of debate, summarized by two hypotheses: the "Hinton" and the "Berlese" models.[1,10,11] The "Hinton" model proposes that holometabolous larvae maintain homology with hemimetabolous nymphs, delaying and internalizing wing development.[12] It asserts that the pupal stage corresponds to the ultimate nymphal instar of the ancestor. The "Berlese" model equates holometabolous pupae with hemimetabolous nymphs and larvae with pre-hatching pronymphs.[10] For years, these contrasting views have coexisted, evolving separately and demanding new evidence for resolution.

Observing the internal structure of insects through the pupal exoskeleton has always been a major obstacle in studying this issue. Davies and Harvey[13] attempted to visualize the internal structures of the crypocephalic and phanerocephalic pupa of a fly *Calliphora vicina* using micro-computer tomography (micro-CT) technology, a non-destructive imaging technique that uses X-rays to generate high-resolution tomographic images.[14,15] Their results effectively illustrate the inheritance of larval organs in the pupa.[13] With the aid of micro-CT, the internal organ changes during the complete metamorphosis of *Chrysopa pallens*, *Chrysomela populi*, and *Trichogramma telengai* were detailed.[16–18] These studies demonstrated that many organs, such as the digestive system and tracheal system, originate in the larval stage and only undergo morphological changes.[16–18] However, these results are derived from holometabolous insects, lacking comparisons with insects of different metamorphic types, making it difficult to resolve the existing controversies. Wings play a crucial role as indicators of insects

[1]Key Laboratory of Biology of Crop Pathogens and Insects of Zhejiang Province, Institute of Insect Sciences, Zhejiang University, Hangzhou 310058, Zhejiang Province, China
[2]Object Research Systems (ORS) Inc, 760 Saint-Paul St W, Montreal, Quebec H3C 1M4, Canada
[3]These authors contributed equally
[4]Lead contact
*Correspondence: zhouhang716@zju.edu.cn (H.Z.), lifei18@zju.edu.cn (F.L.)
https://doi.org/10.1016/j.isci.2024.110898

transitioning into the metamorphosis phase. Comparative analysis of the developmental processes of wings across different insect orders will contribute to a clearer understanding of the corresponding developmental stages among insects.

Exploring the molecular foundations behind developmental patterns can help identify the general principles driving phenotypic evolution.[19] Cardoso-Moreira et al.[19] performed a comprehensive analysis of the evolutionary patterns of gene expression in mammalian organs throughout developmental stages via RNA sequencing (RNA-seq).[19] Similarly, a comparative transcriptomic analysis of two distinct neopteran insects, *Blattella germanica* and *Drosophila melanogaster*, across various developmental stages, revealed divergent gene expression patterns within hormone-related pathways.[20] Their work exemplifies the potential application of developmental RNA-seq in elucidating the correspondence across developmental stages. Except for the model organism *D. melanogaster*,[21] RNA-seq data across continuous prepupal to pupal stages remain scarce for holometabolous insects. The prepupal stage, a critical transition from larva to pupa, has been overlooked.

To investigate the developmental correspondences between hemimetabolous and holometabolous insects, we selected three species from different insect orders: the migratory locust (*Locusta migratoria*, Orthoptera), the harlequin ladybird (*Harmonia axyridis*, Coleoptera), and the diamondback moth (*Plutella xylostella*, Lepidoptera). Using micro-CT, we compared the wing development process during juvenile stages. Additionally, we employed developmental RNA-seq to perform a clustering analysis of gene expression patterns across various larval stages in four insect species, including the model organism *Drosophila melanogaster*. Our goal was to uncover potential commonalities underlying their distinct metamorphic strategies on morphological and molecular levels during juvenile development.

RESULTS

Wing growth processes

L. migratoria, a representative hemimetabolous insect, and two holometabolous species, the harlequin ladybird, *H. axyridis*, and the diamondback moth, *P. xylostella*, were selected to examine the wing development processes during their metamorphosis stages. As complete metamorphosis initiates at the anaphase of the final larval instar, the prepupa, we subdivided the prepupal stages into more detailed segments (Figure 1A). The cuticle's opacity hinders direct observation of internal structures; hence, we employed micro-CT to generate tomographic images, reconstructing the 3D wing structures for observation and quantitative analysis (Figure 1B). Our analysis focused on overall changes, deliberately avoiding further segmentation within the wing areas. At each time point, 4–5 samples were obtained for micro-CT scanning, and the three samples with the best scanning results were selected for subsequent analysis. We retained 69 samples representing various developmental stages, resulting in the collection of 84,623 reconstructed CT images, which constituted approximately 227 gigabytes (GiB) of data (Tables S1–S3).

Considering the increasing body size of locusts with each instar, we normalized wing volume against the width of the prothorax (Figure S1). In the first instar (N1), the fore- and hindwing pads were bifurcated but merged by the second instar (N2), subsequently enlarging and extending toward the abdomen (Figure 1C). No significant volume change occurred between the first (N5d1) and third days of the fifth instar (N5d3) (forewings: $t = -1.370$, $df = 10$, $p = 0.208$;hindwings: $t = -0.050$, $df = 10$, $p = 0.961$) (Figure 1D), indicating a temporary growth plateau. Growth resumed thereafter, peaking just before eclosion (N5d5) (Figure 1D). Throughout the entire nymphal development process, the volume increase of the forewings and hindwings reached 88.21% and 93.72% of their final volume, respectively (Figure 1D).

In the prepupal stages of ladybirds, distinctive grooves developed on wing surfaces, and volume increased progressively (Figure 2E). The cross-sectional analysis reveals a progressive increase in the thickness of both the fore- and hindwings during the prepupal stage, culminating in a vertical folding at 20 h after prepupation (PP5) (Figure S2B). At the same time, wing volumes equaled those at 1-day post-pupation (P1) (forewings: $t = 0.057$, $df = 10$, $p = 0.955$; hindwings: $t = 1.614$, $df = 10$, $p = 0.138$) (Figure 1F). Minimal change in wing volume was observed from P1 to 2 days post-pupation (P2) (forewings: $t = -0.095$, $df = 10$, $p = 0.926$; hindwings: $t = -0.299$, $df = 10$, $p = 0.771$), followed by rapid growth (Figure 1F). The cross-sectional view of the pupa shows that the process of increasing wing thickness mainly occurs from P3 to P4 (Figure S2D). The volume of fore- and hindwings increased by 94.76% and 91.35%, respectively, from prepupa to the final day of pupa (Figure 1F). Similarly, the diamondback moth exhibited comparable wing development (Figures 1G–1S, 2F, and S2H), with relative increases of 89.19% and 89.86% in fore- and hindwings, including a stagnation phase during the prepupal to pupal transition (forewings: $t = -1.005$, $df = 10$, $p = 0.316$; hindwings: $t = -0.299$, $df = 10$, $p = 0.771$) (Figure 1H). These results suggest that the prepupal and pupal stages of ladybirds and diamondback moths closely resemble the complete nymphal stage of locusts, encompassing the principal growth phase of wings with a transient plateau following the final molt.

Developmental transcriptomes

To assess if morphological correspondence correlates with gene expression patterns and to substantiate the "Hinton" hypothesis of parallelism between holometabolous larval stages and ancestor nymphal stages,[12] we conducted developmental RNA-seq analyses on three insect species and *D. melanogaster*, including extra larval samples from holometabolous insects (Figure 2A). RNA-seq data were generated for 93 samples spanning the continuous developmental stages of *L. migratoria*, *H. axyridis*, and *P. xylostella*. A total of 1,056,511,608 read pairs were obtained, as detailed in Tables S4–S6. The *D. melanogaster* RNA-seq data were obtained from a previous study (Table S7).[21] Based on the variance-stabilized counts of 3,180 single-copy orthologs (SC-OGs) and 509 SNAP-orthologs across four species, global principal-component analysis (PCA) showed that all samples were clustered according to their species type in the global PCA (Figure 2B).

The quantity of differentially expressed genes (DEGs) between adjacent developmental stages signifies the magnitude of developmental transformations.[19,22] In the developmental trajectory of *L. migratoria*, a pronounced peak in the number of DEGs emerged when comparing the 5th instar nymphs (N5) to the 4th instar nymphs (N4) (Figure 3A). However, the Gene Ontology (GO) annotations of upregulated genes

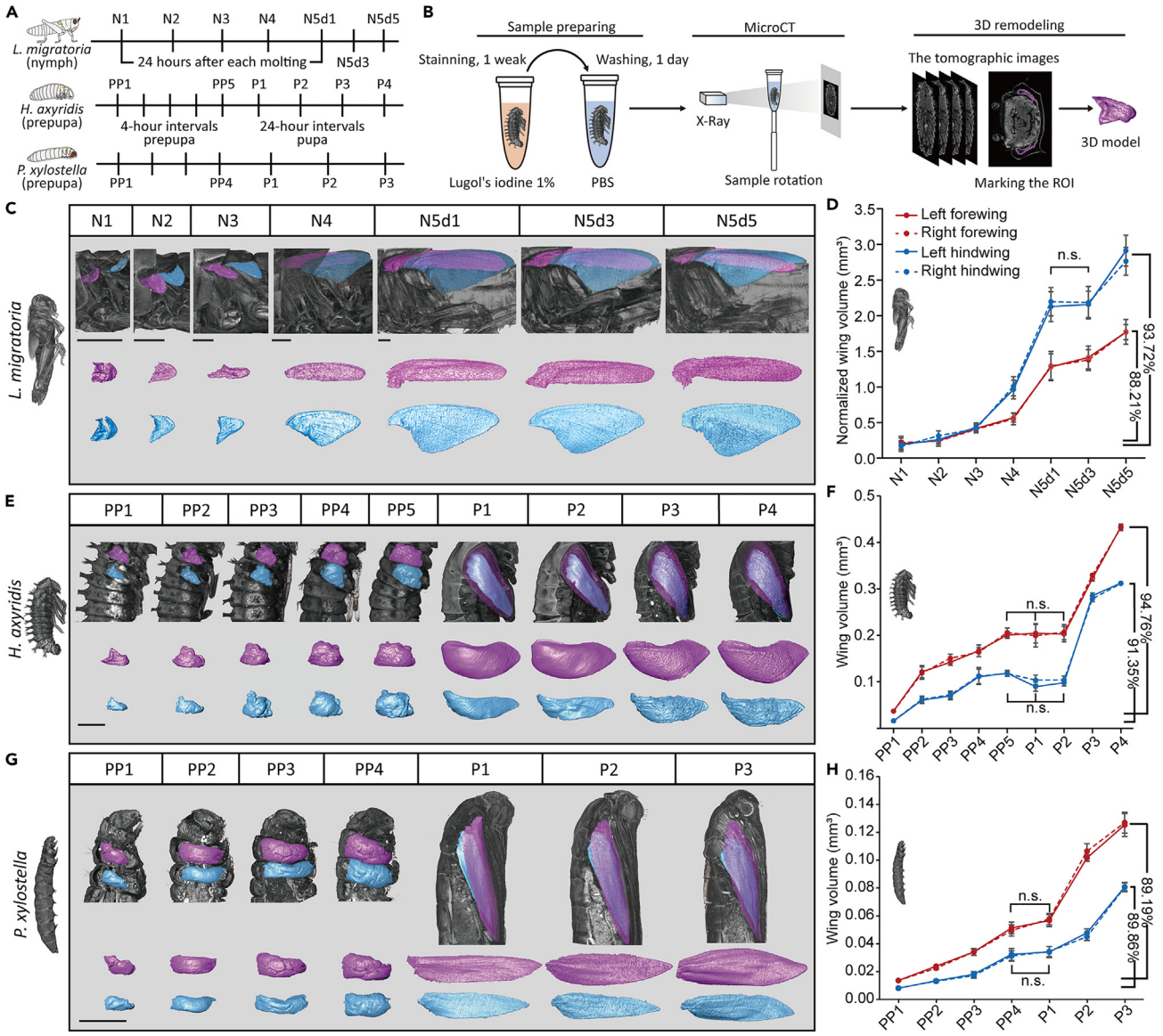

Figure 1. Comparison of the wing growth process

(A) Schematic diagram of the sampling time points. N1 to N5 refers to the nymphal instars of *Locusta migratoria*. Samples from each instar were collected 24 h after molting. In the case of *Harmonia axyridis* and *Plutella xylostella*, PP refers to prepupa, whereas P refers to pupa. Samples were collected every 4 h after entering the prepupal stages and every 24 h after entering the pupal stages.

(B) Experimental design for the observation of inner structures using micro-CT.

(C) Process of wing morphogenesis during the nymphal stage in *L. migratoria*. Wing size was normalized using the prothorax width.

(D) Normalized wing volume of *L. migratoria* during juvenile stages. *L. migratoria* wing volumes were normalized against the width of the prothorax (Figure S1).

(E) Wing morphogenesis process from prepupal to pupal stages in *H. axyridis*.

(F) Wing volume of *H. axyridis* from prepupal to pupal stages.

(G) Wing morphogenesis process from prepupal to pupal stages in *P. xylostella*.

(H) Wing volume of *P. xylostella* from prepupal to pupal stages. The displayed wing models represent the intermediate state of three replicates. The fore- and hindwings are marked in purple and blue, respectively. Scale bars: 1 mm. Statistical analysis: n.s. = nonsignificant ($p > 0.05$). All the data are represented as mean ± SEM.

revealed that significant gene enrichment was absent in developmental biology processes, except for terms related to epidermal development (Figure 3A). Conversely, the GO annotations for upregulated genes between the 4th and 3rd instar nymphs (N4 and N3) highlighted significant enrichment in genes associated with the reproductive, digestive, and internal circulatory systems (Figure 3E). This suggests that the 4th instar represents a pivotal phase in the maturation of critical adult organs, in locusts.

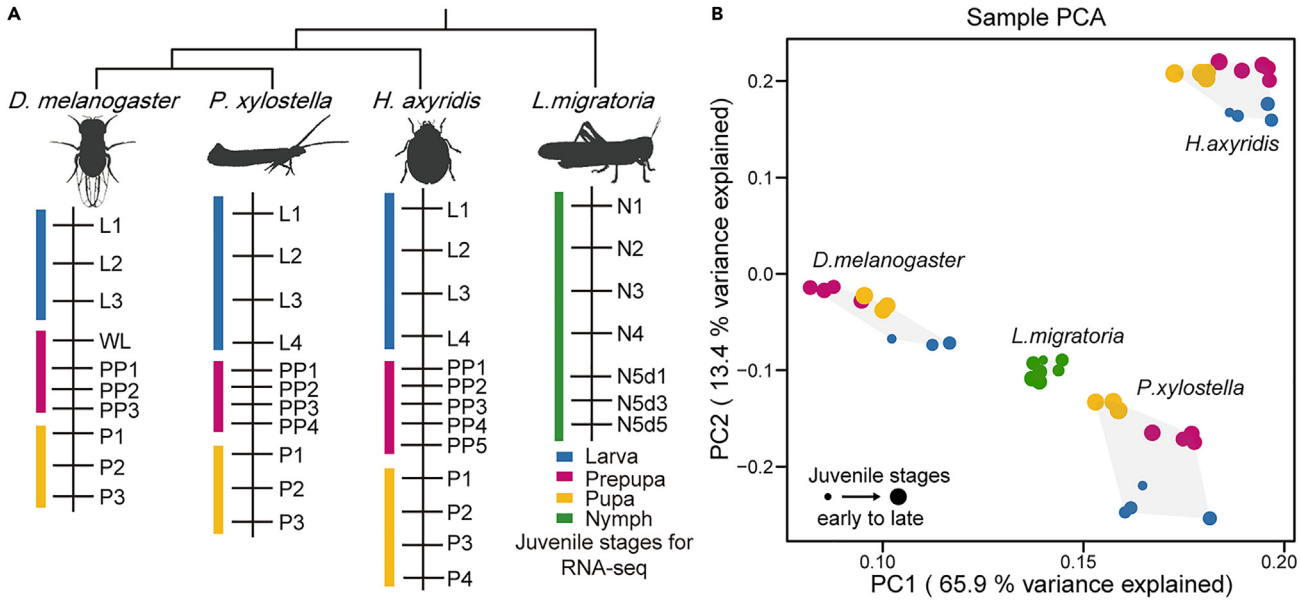

Figure 2. Transcriptomes of developmental stages across insects

(A) Sampling stages of developmental transcriptomes. The sampling time points of prepupae and pupae are the same as those for the micro-CT experiments. Larvae samples of holometabolous insects were collected 24 h after molting at each instar. Three replicates were obtained for each time point.

(B) Sample principal-component analysis (PCA) plot based on variance-stabilized counts of 3,680 1:1 orthologs across four species. Each dot represents the median across three replicates. Developmental stages were marked with different colors.

In *H. axyridis*, transcriptional changes exhibited fluctuations, but the number of DEGs peaked in the comparison between the 48 h and 24 h post-pupation (P2 and P1) (Figure 3B). GO terms related to organ development were most enriched in the comparison between 4 h after prepupation and the 4th instar (PP1 and L4) (Figure 3E), whereas the comparison between P1 and late prepupation (PP5) also showed enrichment of terms such as appendage, eye, and sensory organ development. In *P. xylostella* and *D. melanogaster*, the number of DEGs peaked during the two transformation periods: from larva to prepupa and from prepupa to pupa (Figures 3C and 3D). Developmental-related GO terms were enriched during these same periods (Figure 3E). These findings suggest that the most substantial transcriptional changes associated with metamorphosis development in holometabolous insects occur during the larval-to-prepupal and prepupal-to-pupal transitions.

Developmental correspondences of juvenile stages

To leverage gene expression patterns in investigating the correspondence of developmental stages, we initially applied the *Z* SCORE algorithm to standardize gene expression levels across a temporal sequence. Based on standardized expression level, global PCA sorted different insect instars into three clusters (Figure 4A). The larvae of ladybirds, fruit flies, and diamondback moths grouped together, whereas the nymphal stages of locusts clustered with the prepupal and pupal stages of the other three insects (Figure 4A).

To validate this clustering, we applied uniform manifold approximation and projection (UMAP), a dimensionality reduction algorithm commonly used in single-cell clustering analysis,[23,24] combined with K-means algorithm. UMAP clustering results closely mirrored those of PCA, except for a reclassification of the fruit fly's PP1 and the moth's PP3 (Figure 4B). Both UMAP and PCA clustering analyses distinctly grouped the larvae of ladybirds, moths, and fruit flies (Figures 4A and 4B). Hierarchical clustering supported these results with "average" method. The larvae of holometabolous insects were distinct from the other juvenile stages (Figure 4C). These findings suggest a closer similarity in gene expression patterns between the prepupal and pupal stages of holometabolous insects and the nymphal stages of hemimetabolous insects, whereas the primary larval stages exhibit unique gene expression pattern distinct from these stages.

Relationships between evolution and gene expression dynamics

To further investigate the relationship between temporal dynamics of gene expression and species evolution, we first calculated the time-specificity index (Tau value)[25] for 1:1 orthologs across four species. A higher Tau value indicates a gene with more stage-specific expression, whereas a lower Tau value suggests a gene with more ubiquitous expression across developmental stages.[19,25] Throughout the juvenile stages, the distribution of Tau values for 1:1 orthologs in *L. migratoria* exhibited two major peaks within 0.1–0.3 (Figure 5). *H. axyridis* and *P. xylostella* showed peaks within 0.3–0.5, whereas *D. melanogaster* exhibited a higher peak within 0.4–0.6 (Figure 5). As the timing of species divergence becomes more recent, we observe a significant increase in the median Tau value (Table 1; Table S8), accompanied by an increase in the number of time-specific orthologs (Tau $\geq$0.85). In *L. migratoria*, the number of time-specific genes peaks in the 3rd instar nymphs (N3) (Figure S3A). *H. axyridis* exhibits two peak expression periods: 1st instar larvae (L1) and P2 (Figure S3B). For the remaining two insects, the peak

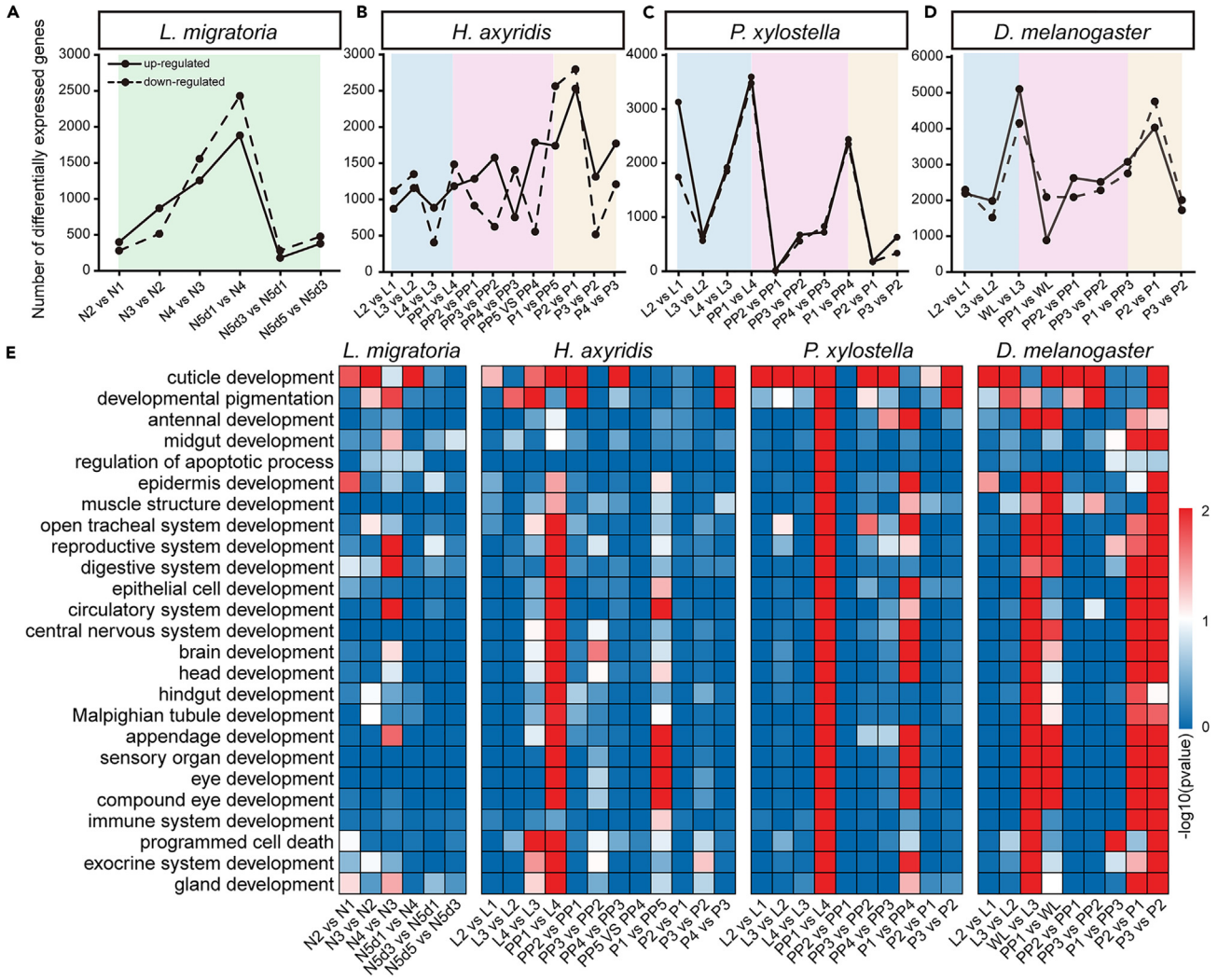

Figure 3. Periods of greater transcriptional change

(A–D) Number of differential expressed genes between adjacent stages in each insects (|log2fold change| > 1). Solid line refers to genes that increase in expression, and dashed line refers to expression-decreased genes. Developmental stages were marked with different colors as shown in Figure 1.

(E) The enrichment of terms related to development process among the biological process category in the Gene Ontology annotations.

number occurs on P1 (Figures S3C and S3D). These results suggest a trend toward temporally specific expression of genes, transitioning from hemimetabolous to holometabolous insects. Temporal-specific genes are predominantly observed in the early phase of the holometabolous pupa.

To assess whether genes exhibiting different expression patterns in holometabolous insects face distinct evolutionary selection pressures, we first categorized the expression patterns of 1:1 orthologs during their juvenile phase. These patterns were divided based on whether there was high expression solely in the larval stages (early-expressed) or exclusively during the prepupal or pupal stages (late-expressed) (Figure 6A). We then calculated the ratio of non-synonymous to synonymous substitution rates (Ka/Ks) for these genes' coding sequences (CDS), as well as the ratio of non-coding nucleotide substitution to neutral substitution rates (Kn/Ks) for their upstream non-coding sequences (Figure 6B).

Among these three holometabolous insects, all CDSs used for Ka/Ks calculation exhibited values less than 1, indicating that these genes are under purifying selection. However, the median Ka/Ks of CDSs late-expressed was significantly higher than that of genes early-expressed (Figures 6C–6E; Table S9). Although no substantial differences were observed in the Ka/Ks of highly early-expressed genes across the three holometabolous species, the median Ka/Ks of late-expressed genes gradually increased with more recent insect species divergence times (Figures S4A and S4B; Table S9). These results suggest that genes highly expressed during metamorphosis stages have retained more non-synonymous substitutions compared to larval-biased genes, and the accumulation of such non-synonymous changes tends to be more pronounced in lineages with more recent divergence times across insect species.

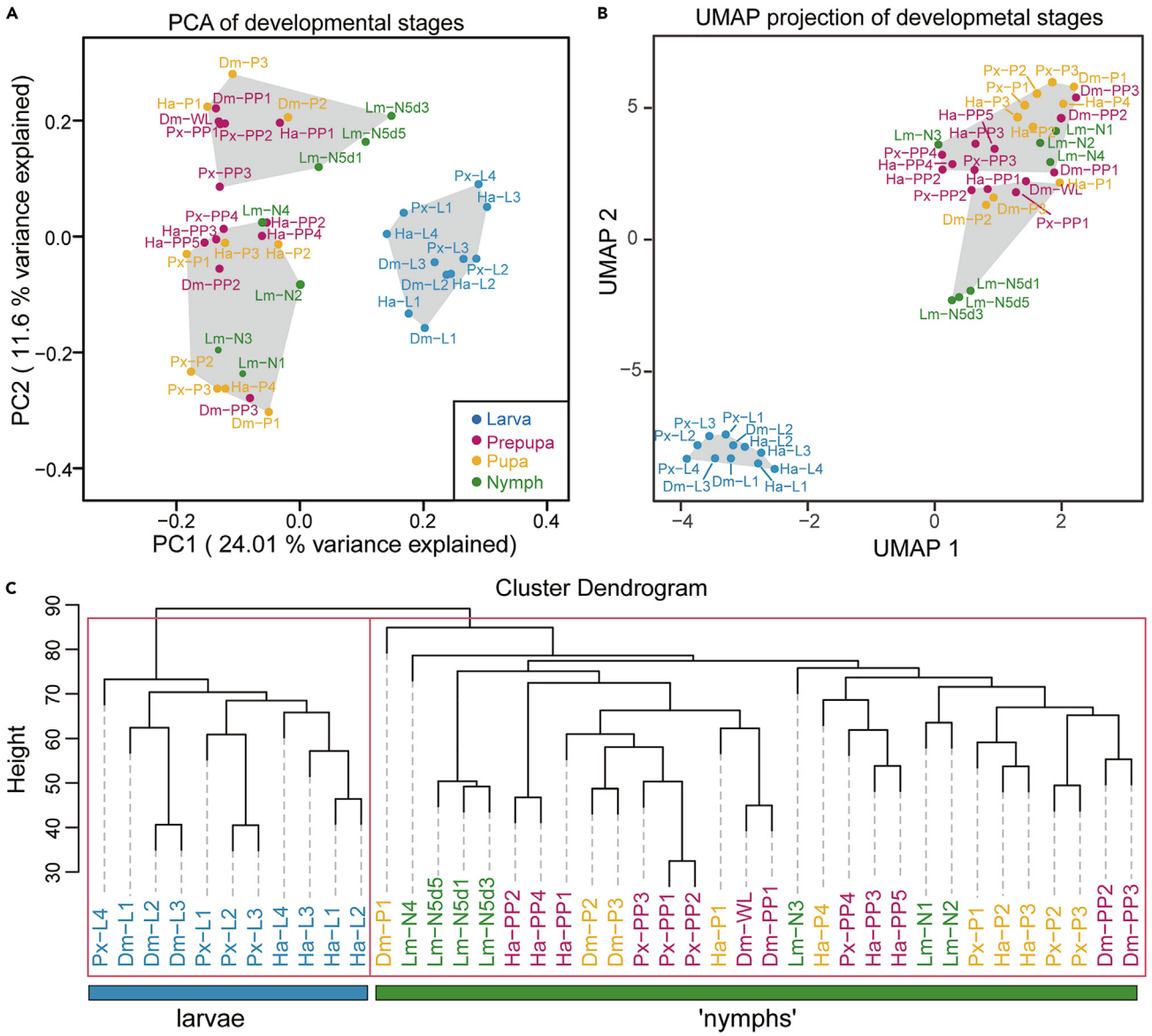

Figure 4. Correspondence of juvenile stages

(A) Sample principal-component analysis (PCA) plot based on variance-stabilized counts of 3,689 1:1 orthologs. The median value of replicates was standardized across developmental stages using *Z* SCORE algorithm.

(B) Uniform manifold approximation and projection (UMAP) of developmental stages, based on the standardized expression level. After dimensionality reduction with PCA and UMAP, the data were subjected to cluster analysis using the K-means algorithm. The gray areas in the figures represent different clusters. Developmental stages were marked with different colors as shown in Figure 1.

(C) Hierarchical clustering of gene expression patterns across different developmental stages with "average" method. The red box indicates two distinct groups.

The median Kn/Ks for non-coding sequences of late-expressed genes was significantly higher than that of early-expressed genes across all species (Figures 6F–6H; Table S10). Unlike the Ka/Ks of CDS, the median Kn/Ks of both early- and late-expressed genes exhibited a gradual increase with more recent order divergence times (Figures 4C and 4D; Table S10).

DISCUSSION

Our integrated analysis of morphological and transcriptomic data across juvenile stages in the locust, harlequin ladybird, and diamondback moth revealed striking commonalities of prepupa/pupa and nymphal stages underlying the distinct metamorphic strategies employed by these representative hemimetabolous and holometabolous insects. By combining micro-CT imaging and 3D remodeling to track wing morphological changes with RNA-seq for developmental transcriptome profiling, we uncovered parallels in wing development processes

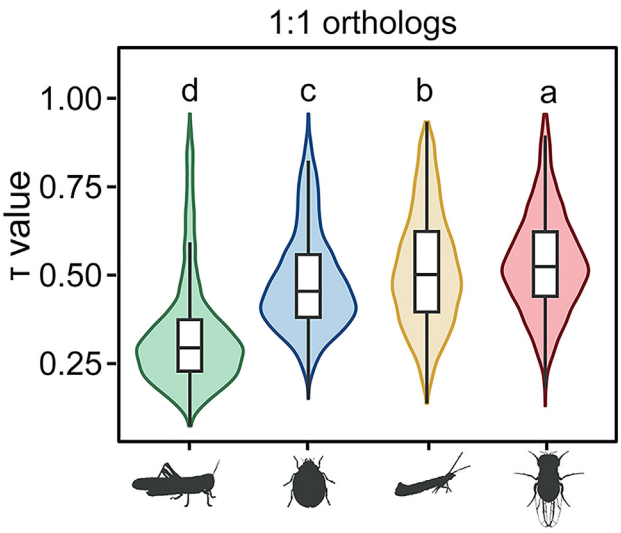

Figure 5. Comparison of gene expression dynamics across insects

Distribution of time-specificity index. A higher Tau value indicates a gene with more time-specific expression, whereas a lower Tau value suggests a more ubiquitously expressed gene. The *p* values of two-sided Wilcoxon rank-sum test are provided in Table S8.

and gene expression dynamics around the nymphal/pupal transition shared between locusts and the two holometabolous species studied. Although there has been microscopic observation of the wing development process in Lepidopteran insects previously,[26,27] a crucial stage, the prepupal phase, was overlooked. Our findings highlight this phase as a key transition from wing buds to adult wings, characterized by dramatic morphological changes.

We observed a transient plateau in wing growth during the final molting of three insect species. In the prepupal stage of the harlequin ladybird and the diamondback moth, the wings developed distinct grooves and exhibited a highly folded appearance (Figures S2 and S3), suggesting that the wings in the early pupal phase are acquired through the unfolding of wings in the later prepupal stage, resulting in minimal volumetric changes. During the transition from the prepupal to the pupal stages, two holometabolous insects undergo over 88% of their wing volume growth. This growth pattern closely mirrors the changes observed in the wing size of locusts during their nymphal phases. These findings highlight the parallels in wing growth between holometabolous insects in their transition from prepupa to pupa and hemimetabolous insects during their nymphal stages, reinforcing the "Berlese" hypothesis, which posits the pupa as the ancestral nymphal stage.[11]

The results from three types of clustering all demonstrate that the gene expression patterns during the holometabolous larval stages are relatively independent and cannot be grouped together with the hemimetabolous nymphal stages. In contrast, the gene expression patterns in the holometabolous prepupal and pupal stages show greater similarity to those of hemimetabolous nymphs. These findings present a clear divergence from the "Hinton" hypothesis but align more closely with the "Berlese" hypothesis.[11,12,28] By comparing the function of transcription factors Broad and Krüppel homolog 1 across insects, Ishimaru et al.[28] assumed that hemimetabolous pronymph, nymph, and penultimate nymph stages correspond to holometabolous larva, last instar larva, and pupa, respectively. In contrast to our findings, their study did not divide the last instar larval stage into greater detail. However, gene expression patterns in the early fourth instar larvae also differed from those observed during the prepupal or pupal stages across holometabolous insects. The gene expression patterns from the prepupal to pupal stages do not exhibit a continuous change along a uniform trend. The clustering algorithms segregated the different phases of the prepupae, pupae, and nymphs into two distinct groups (Figure 4). This could result from non-continuous gene expression driving morphogenesis during the transition from the prepupa to pupa (Figures 3B–3E), marked by periodic activation, leading to discontinuous wing growth.[29,30]

Table 1. Number of time-specific genes

Species	1:1 orthologs	All protein-coding genes
L. migratoria	56	489
H. axyridis	73	1,556
P. xylostella	109	2,583
D. melanogaster	142	1,653

Genes exhibiting a Tau value greater than or equal to 0.85 are considered to demonstrate temporal-specific expression patterns. The Tau indexes are provided in Data S4.

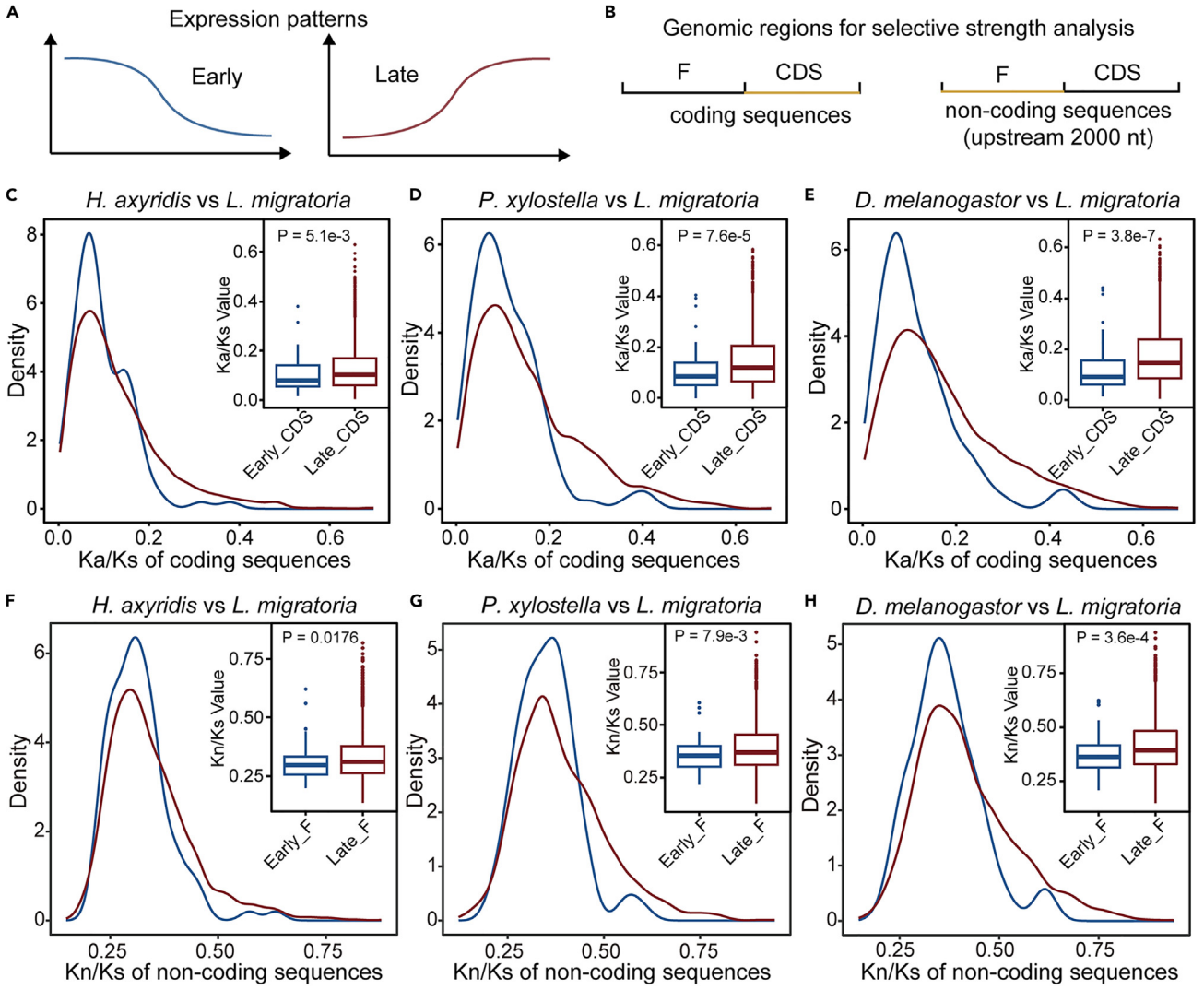

Figure 6. Relationship between gene expression patterns and selective pressures

(A) Two major expression patterns were selected: the first one where genes are highly expressed only during the larval stages (Early) and the second one where genes are highly expressed only during the prepupal or pupal stage (Late).

(B) Genomic regions for selective pressure analysis. The coding sequences (CDSs) were utilized for calculating the ratio of non-synonymous to synonymous substitution rates (Ka/Ks), whereas the upstream 2000 nt non-coding regions were employed for estimating the ratio of non-coding nucleotide substitution to neutral substitution rate (Kn/Ks). Orthologs from *L. migratoria* served as the reference in these calculations.

(C–E) Ka/Ks density of CDS in holometabolous insects.

(F–H) Kn/Ks density of upstream non-coding regions in holometabolous insects. The calculation for Ka, Ks, and Kn is detailed in Data S5–S16. Results from the two-sided Wilcoxon rank-sum test are provided in Tables S9 and S10.

The median time-specificity indexes of *L. migratoria* during juvenile stages were significantly lower than those of the other three holometabolous insects, and the indexes increased with more recent species divergence times (Figure 5). This suggests a reduction in pleiotropic effects for these orthologs, and a shift toward more stage-specific functions.[31] These results may be attributed to a relaxation of functional constraints and increased adaptability.[32,33] Consistent with the selection pressure analyses, the Kn/Ks ratio in non-coding regions exhibited an upward trend with more recent divergence times. These regions encompass potential promoters and untranslated regions (UTRs), which play crucial roles in regulating gene expression and translation. The accumulation of non-coding nucleotide substitutions in these regions could contribute to the observed increase in temporal specificity of gene expression. In contrast to the non-coding regions, there were no significant differences in the Ka/Ks ratios of early-expressed genes among the three holometabolous insects. However, the median Ka/Ks of late-expressed genes exhibited a gradual increase with more recent divergence times (Figures S4A and S4B). This result indicates an association between the pupation behavior and the accumulation of non-synonymous mutations in these genes.

Over all, our study does not support the "Hinton" hypothesis. Yet, the evidence is more consistent with the "Berlese" hypothesis, based on both morphological observations and gene expression patterns. We propose that the transition from prepupal to pupal stages in holometabolous insects evolved from the nymphal stages of their hemimetabolous ancestors. With more recent insect species divergence, juvenile stage gene expression showed increasing stage-specificity. Genes highly expressed in prepupal or pupal stages accumulated more non-synonymous substitutions and non-coding nucleotide substitution rates. Our study contributes insights into the origins of complete metamorphosis by directly comparing gene expression patterns at different insect stages and combining morphological quantification references, offering reliable evidence for the correspondence between different developmental stages of holometabolous insects and their ancestors and clarifying the evolution trend of gene expression dynamics during the juvenile stages of neopteran insects.

Limitations of the study

It is important to note that our conclusions are currently restricted to these species examined, which were specifically selected due to their biological significance and experimental tractability. Future investigations across a broader taxonomic sample are still needed to fully elucidate the evolutionary origins and diversification of metamorphosis within insects. Unlike mammals, a common issue arises when dealing with a wide range of insect species: the shortage of single-copy genes. This means that the genes retained may not fully represent the developmental state of insects. Thus, when incorporating more species, it becomes especially important to carefully select marker genes for developmental stage clustering analysis.

RESOURCE AVAILABILITY

Lead contact

Further information and requests for resources and reagents should be directed to and will be fulfilled by the lead contact, Professor Fei Li (lifei18@zju.edu.cn).

Materials availability

This study did not generate any new unique reagents.

Data and code availability

Data

All micro-CT images can be acquired from InsectBase v2.0: http://v2.insect-genome.com/Micro-CT. Quantitative data on wing volumes of different insects can be found in Data S1–S3. RNA-seq raw data have been deposited in NCBI, and the accession numbers are listed in Tables S1–S4. The expression matrix of different insects is available in Data S4.

Code

This study does not report the original code. General statistics and plots were done in R.[34] Plots were created using the R packages clusterprofiler,[35] ggplot2 (v3.4.4),[36] dplyr (v1.1.4),[37] Mfuzz, (v2.62.0),[38] gridExtra (v2.3),[39] and reshape2 (v1.4.4).[40] Code for RNA-seq and clustering analysis[41] can be acquired from https://github.com/HangZhou716/Developmental-Origin.

Additional information requests

Any additional information required to reanalyze the data used in this study is available from the lead contact upon request.

ACKNOWLEDGMENTS

This project was supported by the National Key R&D Program of China (grant numbers 2021YFD1400100 and 2021YFD1400101), the National Natural Science Foundation of China (grant number 32102271), and the China Postdoctoral Science Foundation (grant number 2022T150579). We acknowledge Engineer Chaogang Xin (Testing Center of the College of Agriculture and Biotechnology, Zhejiang University) for providing technical support in the field of micro-CT. We are grateful to Object Research Systems (ORS) Inc. for granting us long-term usage permissions for Dragonfly software.

AUTHOR CONTRIBUTIONS

F.L. and H.Z. supervised the project. H.Z., R.S., and F.L. wrote the manuscript. H.Z. and R.S. designed all the experiments. R.S. carried the micro-CT screening. H.Z. carried the omics analysis. H.Z., R.S., Y.X., C.Z., and J.T. collected insect samples and performed RNA-seq experiments. D.J., X.C., Y.M., and F.L. contributed to discussion and data presentation. Z.C. collected the source data of micro-CT and provided technical support.

DECLARATION OF INTERESTS

The authors declare no competing interests.

STAR★METHODS

Detailed methods are provided in the online version of this paper and include the following:

- KEY RESOURCES TABLE
- EXPERIMENTAL MODEL AND STUDY PARTICIPANT DETAILS
  - Insect samples
- METHOD DETAILS

- Micro-CT sample labeling
- Sample holder
- Micro-CT scanning
- Image reconstruction
- 3D structure remodeling
- RNA extraction and sequencing
- RNA-seq data processing
- Time-specificity index
- Gene expression patterns
- Selective pressure

- QUANTIFICATION AND STATISTICAL ANALYSIS

SUPPLEMENTAL INFORMATION

Supplemental information can be found online at https://doi.org/10.1016/j.isci.2024.110898.

Received: April 26, 2024
Revised: July 25, 2024
Accepted: September 4, 2024
Published: September 17, 2024

REFERENCES

1. Sehnal, F., Svácha, P., and Zrzavy, J. (1996). Postembryonic reprogramming of gene expression in amphibian and insect cells. In Metamorphosis, L.I. Gilbert, J.R. Tata, and B.G. Atkinson, eds. (Academic), pp. 3–58.
2. Erezyilmaz, D.F. (2006). Imperfect eggs and oviform nymphs: a history of ideas about the origins of insect metamorphosis. Integr. Comp. Biol. *46*, 795–807.
3. Heming, B.S. (2018). Insect Development and Evolution (Cornell University Press).
4. Istock, C.A. (1967). The evolution of complex life cycle phenomena: an ecological perspective. Evolution *21*, 592–605.
5. Rainford, J.L., Hofreiter, M., Nicholson, D.B., and Mayhew, P.J. (2014). Phylogenetic distribution of extant richness suggests metamorphosis is a key innovation driving diversification in insects. PLoS One *9*, e109085.
6. Ten Brink, H., de Roos, A.M., and Dieckmann, U. (2019). The evolutionary ecology of metamorphosis. Am. Nat. *193*, E116–E131.
7. Condamine, F.L., Clapham, M.E., and Kergoat, G.J. (2016). Global patterns of insect diversification: towards a reconciliation of fossil and molecular evidence? Sci. Rep. *6*, 19208.
8. Misof, B., Liu, S., Meusemann, K., Peters, R.S., Donath, A., Mayer, C., Frandsen, P.B., Ware, J., Flouri, T., Beutel, R.G., et al. (2014). Phylogenomics resolves the timing and pattern of insect evolution. Science *346*, 763–767.
9. Belles, X. (2019). The innovation of the final moult and the origin of insect metamorphosis. Philosophical Transactions of the Royal Society B *374*, 20180415.
10. Jindra, M. (2019). Where did the pupa come from? The timing of juvenile hormone signalling supports homology between stages of hemimetabolous and holometabolous insects. Philosophical Transactions of the Royal Society B *374*, 20190064.
11. Truman, J.W., and Riddiford, L.M. (2019). The evolution of insect metamorphosis: a developmental and endocrine view. Philosophical Transactions of the Royal Society B *374*, 20190070.
12. Hinton, H.E. (1963). The origin and function of the pupal stage. In Proceedings of the Royal Entomological Society of London. Series A, General Entomology, *38*Proceedings of the Royal Entomological Society of London. Series A, General Entomology (Wiley Online Library), pp. 77–85.
13. Davies, K., and Harvey, M.L. (2013). Internal morphological analysis for age estimation of blow fly pupae (Diptera: Calliphoridae) in postmortem interval estimation. J. Forensic Sci. *58*, 79–84.
14. Ritman, E.L. (2011). Current status of developments and applications of micro-CT. Annu. Rev. Biomed. Eng. *13*, 531–552.
15. Schoborg, T.A., Smith, S.L., Smith, L.N., Morris, H.D., and Rusan, N.M. (2019). Micro-computed tomography as a platform for exploring *Drosophila* development. Development *146*, dev176685.
16. Zhao, C., Wang, M., Gao, C., Li, M., Zhang, K., Yang, D., and Liu, X. (2022). Evolution of holometaboly revealed by developmental transformation of internal thoracic structures in a green lacewing *Chrysopa pallens* (Neuroptera: Chrysopidae). Insect Sci. *29*, 767–782.
17. Makarova, A.A., Veko, E.N., and Polilov, A.A. (2021). Metamorphosis of the central nervous system of *Trichogramma telengai* (Hymenoptera: Trichogrammatidae). Arthropod Struct. Dev. *60*, 101005.
18. Ge, S.Q., Hua, Y., Ren, J., Ślipiński, A., Heming, B., Beutel, R., Yang, X.K., and Wipfler, B. (2015). Transformation of head structures during the metamorphosis of *Chrysomela populi* (Coleoptera: Chrysomelidae). Arthropod Syst. Phylogeny *73*, 129–152.
19. Cardoso-Moreira, M., Halbert, J., Valloton, D., Velten, B., Chen, C., Shao, Y., Liechti, A., Ascenção, K., Rummel, C., Ovchinnikova, S., et al. (2019). Gene expression across mammalian organ development. Nature *571*, 505–509.
20. Ylla, G., Piulachs, M.D., and Belles, X. (2018). Comparative transcriptomics in two extreme neopterans general trends in the evolution of modern insects. iScience *4*, 164–179.
21. Graveley, B.R., Brooks, A.N., Carlson, J.W., Duff, M.O., Landolin, J.M., Yang, L., Artieri, C.G., van Baren, M.J., Boley, N., Booth, B.W., et al. (2011). The developmental transcriptome of *Drosophila melanogaster*. Nature *471*, 473–479.
22. Dillman, A.A., Hauser, D.N., Gibbs, J.R., Nalls, M.A., McCoy, M.K., Rudenko, I.N., Galter, D., and Cookson, M.R. (2013). mRNA expression, splicing and editing in the embryonic and adult mouse cerebral cortex. Nat. Neurosci. *16*, 499–506.
23. Becht, E., McInnes, L., Healy, J., Dutertre, C.A., Kwok, I.W.H., Ng, L.G., Ginhoux, F., and Newell, E.W. (2018). Dimensionality reduction for visualizing single-cell data using UMAP. Nat. Biotechnol. *37*, 38–44.
24. McInnes, L., Healy, J., and Melville, J. (2018). Umap: Uniform manifold approximation and projection for dimension reduction. Preprint at arXiv. https://doi.org/10.48550/arXiv.1802.03426.
25. Yanai, I., Benjamin, H., Shmoish, M., Chalifa-Caspi, V., Shklar, M., Ophir, R., Bar-Even, A., Horn-Saban, S., Safran, M., Domany, E., et al. (2005). Genome-wide midrange transcription profiles reveal expression level relationships in human tissue specification. Bioinformatics *21*, 650–659.
26. Iwata, M., Tsutsumi, M., and Otaki, J.M. (2018). Developmental dynamics of butterfly wings: real-time in vivo whole-wing imaging of twelve butterfly species. Sci. Rep. *8*, 16848.
27. Niitsu, S., and Kamito, T. (2021). Morphological and histological examination of short-wing formation in the winter moth *Protalcis concinnata* (Insecta: Lepidoptera, Geometridae). J. Morphol. *282*, 160–168.
28. Ishimaru, Y., Tomonari, S., Watanabe, T., Noji, S., and Mito, T. (2019). Regulatory mechanisms underlying the specification of the pupal-homologous stage in a hemimetabolous insect. Philosophical Transactions of the Royal Society B *374*, 20190225.
29. Ureña, E., Chafino, S., Manjón, C., Franch-Marro, X., and Martín, D. (2016). The Occurrence of the Holometabolous Pupal Stage Requires the Interaction between E93, Krüppel-Homolog 1 and Broad-Complex. PLoS Genet. *12*, e1006020.
30. Ishimaru, Y., Tomonari, S., Matsuoka, Y., Watanabe, T., Miyawaki, K., Bando, T., Tomioka, K., Ohuchi, H., Noji, S., and Mito, T. (2016). TGF-β signaling in insects regulates metamorphosis via juvenile hormone

biosynthesis. Proc. Natl. Acad. Sci. USA *113*, 5634–5639.
31. Winter, E.E., Goodstadt, L., and Ponting, C.P. (2004). Elevated rates of protein secretion, evolution, and disease among tissue-specific genes. Genome Res. *14*, 54–61.
32. Stern, D.L. (2000). Evolutionary developmental biology and the problem of variation. Evolution *54*, 1079–1091.
33. Carroll, S.B. (2005). Evolution at two levels: on genes and form. PLoS Biol. *3*, e245.
34. R Core Team (2014). R. R: A language and environment for statistical computing.
35. Yu, G., Wang, L.G., Han, Y., and He, Q.Y. (2012). clusterProfiler: an R package for comparing biological themes among gene clusters. OMICS A J. Integr. Biol. *16*, 284–287.
36. Wickham, H. (2009). ggplot2: Elegant Graphics for Data Analysis (Springer-Verlag).
37. Wickham, H. (2011). The split-apply-combine strategy for data analysis. J. Stat. Softw. *40*, 1–29.
38. Kumar, L., and Futschik, M.E. (2007). Mfuzz: a software package for soft clustering of microarray data. Bioinformation *2*, 5–7.
39. Auguie, B., and Antonov, A. (2011). gridExtra: Miscellaneous Functions for 'grid' Graphics.
40. Wickham, H. (2007). Reshaping data with the reshape package. J. Stat. Softw. *21*, 1–20.
41. Likas, A., Vlassis, N.J., and Verbeek, J. (2003). The global k-means clustering algorithm. Pattern Recogn. *36*, 451–461.
42. Krueger, F. (2015). TrimGalore: a wrapper tool around Cutadapt and FastQC to consistently apply quality and adapter trimming to FastQ files. https://www.bioinformatics.babraham.ac.uk/projects/trim_galore/.
43. Ranwez, V., Douzery, E.J.P., Cambon, C., Chantret, N., and Delsuc, F. (2018). MACSE v2: toolkit for the alignment of coding sequences accounting for frameshifts and stop codons. Mol. Biol. Evol. *35*, 2582–2584.
44. Zhang, Z. (2022). KaKs_Calculator 3.0: Calculating Selective Pressure on Coding and Non-coding Sequences. Dev. Reprod. Biol. *20*, 536–540.
45. Kim, D., Paggi, J.M., Park, C., Bennett, C., and Salzberg, S.L. (2019). Graph-based genome alignment and genotyping with HISAT2 and HISAT-genotype. Nat. Biotechnol. *37*, 907–915.
46. Li, H., Handsaker, B., Wysoker, A., Fennell, T., Ruan, J., Homer, N., Marth, G., Abecasis, G., and Durbin, R.; 1000 Genome Project Data Processing Subgroup (2009). The Sequence Alignment/Map format and SAMtools. Bioinformatics *25*, 2078–2079.
47. Liao, Y., Smyth, G.K., and Shi, W. (2014). featureCounts: an efficient general purpose program for assigning sequence reads to genomic features. Bioinformatics *30*, 923–930.
48. Cantalapiedra, C.P., Hernández-Plaza, A., Letunic, I., Bork, P., and Huerta-Cepas, J. (2021). eggNOG-mapper v2: functional annotation, orthology assignments, and domain prediction at the metagenomic scale. Mol. Biol. Evol. *38*, 5825–5829.
49. Emms, D.M., and Kelly, S. (2019). OrthoFinder: phylogenetic orthology inference for comparative genomics. Genome Biol. *20*, 1–14.
50. Steenwyk, J.L., Goltz, D.C., Buida, T.J., 3rd, Li, Y., Shen, X.X., and Rokas, A. (2022). OrthoSNAP: A tree splitting and pruning algorithm for retrieving single-copy orthologs from gene family trees. PLoS Biol. *20*, e3001827.
51. Andrews, S. (2017). FastQC: a quality control tool for high throughput sequence data (Cambridge).
52. Zhou, H., Ma, Z., Wang, Z., Yan, S., Wang, D., and Shen, J. (2021). Hedgehog signaling regulates regenerative patterning and growth in *Harmonia axyridis* leg. Cell. Mol. Life Sci. *78*, 2185–2197.
53. Mei, Y., Jing, D., Tang, S., Chen, X., Chen, H., Duanmu, H., Cong, Y., Chen, M., Ye, X., Zhou, H., et al. (2022). InsectBase 2.0: a comprehensive gene resource for insects. Nucleic Acids Res. *50*, D1040–D1045.
54. Love, M.I., Huber, W., and Anders, S. (2014). Moderated estimation of fold change and dispersion for RNA-seq data with DESeq2. Genome Biol. *15*, 1–21.
55. Murtagh, F., and Contreras, P. (2017). Algorithms for hierarchical clustering: an overview. II. Wires. Data Min. Knowl. *7*, e1219.

STAR★METHODS

KEY RESOURCES TABLE

REAGENT or RESOURCE	SOURCE	IDENTIFIER
Biological samples		
Locusta migratoria	Zhejiang University. Zhejiang Province	Hang Zhou
Plutella xylostella	Zhejiang University. Zhejiang Province	Hang Zhou
Harmonia axyridis	Zhejiang University. Zhejiang Province	Chaowei Zhang
Deposited data		
RNA-seq data of *Locusta migratoria, Plutella xylostella, and Harmonia axyridis*	This paper	PRJNA973931
Mciro-CT data	This paper	http://v2.insect-genome.com/Micro-CT
RNA-seq data of *Drosophila melanogaster*	NCBI	PRJNA75285
Critical commercial assays		
TruePrep RNA Library Prep Kit for Illumina	Vazyme, Nanjing, China	TR501
RNA isolater Total RNA Extraction Reagent	Vazyme, Nanjing, China	R401-01
Lugol's solution	Sigma-Aldrich	1005671000
Software and algorithms		
R 4.0.4	R Core Team[34]	https://www.r-project.org/
Python version 3.9	Python Software Foundation	https://www.python.org
NRecon	Bruker	https://www.bruker.com/
TrimGalore	Krueger[42]	https://github.com/FelixKrueger/TrimGalore
MACSE	Ranwez et al.[43]	https://github.com/ranwez/MACSE_V2_PIPELINES
KaKs_Caculator	Zhang[44]	https://github.com/lizzhao/Kaks_Calculator
Hisat2	Kim et al.[45]	https://daehwankimlab.github.io/hisat2/
Samtools	Li et al.[46]	https://www.htslib.org/
featureCounts	Liao et al.[47]	https://subread.sourceforge.net/featureCounts.html
eggNOG-mapper	Cantalapiedra et al.[48]	http://eggnog-mapper.embl.de/
Orthofinder	Emms et al.[49]	https://github.com/davidemms/OrthoFinder
OrthoSNAP	Steenwyk et al.[50]	https://github.com/JLSteenwyk/orthosnap
FastQC	Andrew et al.[51]	https://github.com/ChristophRau/wMICA
Other		
SKYSCAN 1272 system	Bruker	https://www.bruker.com/

EXPERIMENTAL MODEL AND STUDY PARTICIPANT DETAILS

Insect samples

Nymphs of *Locusta migratoria* were maintained at 26 ± 1°C and 50% relative humidity, while *Harmonia axyridis* and *Plutella xylostella* were reared at 25 ± 1°C and 75% relative humidity. Larvae and nymphs were collected 24 h post-molting. Prepupae of *H. axyridis* and *P. xylostella* were collected at 4-h intervals following entry into the prepupal phase. Pupae were similarly collected at 24-h intervals upon entering the pupal stage. Developmental stages were verified using a Sony FDR-AX60 video camera. Entry into the prepupal stage for *H. axyridis* larvae was indicated by cessation of movement and a curled posture. For *P. xylostella* larvae, the initiation of cocoon spinning marked the transition to the prepupal stage. The method for determining the commencement of the pupal stage mirrored that used for the prepupal stage. At each time point, 4–5 samples were obtained for Micro-CT scanning, and the 3 samples with the best scanning results were selected for subsequent analysis.

METHOD DETAILS

Micro-CT sample labeling

We adopted the fruit fly labeling method[15] for our study. Carbon dioxide served as the anesthetic for the insects, which were then transferred to 75% ethanol for 1 day. Subsequently, we washed the samples three times with 1 mL of phosphate-buffered saline (PBS) and stained them with 1 mL of standard Lugol's solution for one week. After staining, we performed three additional washes with PBS to eliminate excess Lugol's solution, and the samples were stored in PBS at 25°C until scanning. The scanning process was executed within one week of sample preparation to ensure the precision of morphological and quantitative analyses.

Sample holder

The method for holding samples varied based on the size of the insect specimens. We opted for pipette tips of appropriate sizes for different insect specimens to facilitate sample loading. For larger insects, such as locusts, we utilized a modified 1.5 mL Eppendorf tube as the sample loading apparatus. This involved sealing the pipette tip at a high temperature and then trimming it to the desired length. PBS was introduced into the pipette tip as a buffer solution. The sample was carefully transferred into the pipette tip, and a brush was used to guide it down gently until it adhered to the inner wall, ensuring immobility. To prevent liquid evaporation during prolonged scanning, we sealed the pipette tip's opening with parafilm. Plasticine was used to secure the sample holder to the sample mount, ensuring careful alignment along the mount's long axis to minimize sample movement during rotation.

Micro-CT scanning

The high-resolution 3D X-ray microscopy was conducted using a Skyscan 1272 desktop unit, operated via a Dell desktop workstation. The workstation featured an Intel Xeon Gold 6128 Processor, 128 GB of memory, and an NVIDIA Quadro P4000 graphics card. The SKYSCAN 1272 system facilitated instrument control, measurement planning, and data acquisition. X-ray parameters were set to 45 kV for voltage and 35 μA for current. Image capture employed a 16 MP sCMOS detector, translating X-rays into photons. We adjusted the scanning resolution to its maximum to ensure the inclusion of the entire sample. To mitigate image blurring due to sample rotation, we set random movement correction at 30, and for enhanced signal-to-noise ratio in the images, frame averaging was configured to 6.

Image reconstruction

NRecon (Bruker, v1.7.4) was utilized for generating tomographic images. Reconstruction sensitivity to the features of original images, including brightness and contrast, significantly affects the final results. While slight differences in reconstruction settings may exist for different samples, the general settings encompass image registration, ring artifact correction, and beam-hardening correction. Users can customize these three settings with the NRecon software. During the reconstruction process, we adhered to the default image registration, a ring artifact correction range of 5–10, and a beam-hardening setting of 95%. The information of the reconstructed images can be obtained from Tables S1–S3.

3D structure remodeling

We conducted micro-CT imaging and performed statistical analysis using Dragonfly software (Object Research Systems, version 2022.2.0.1361) on a Dell workstation equipped with an i9-11900 Intel Core processor, 128 GB of memory, and an Nvidia GeForce RTX 3070Ti graphics card. To delineate individual regions of interest (ROIs), we utilized a manual 2D paintbrush tool. The segmentation process involved the use of the Otsu algorithm, facilitating the rapid extraction of high-density areas and minimizing human bias. This algorithm automatically identified and outlined high-density regions based on the grayscale distribution within the brushed area. Following ROI delineation, the software directly calculated the corresponding tissue volumes. Wing volumes of different insects are available in Data S1–S3. These ROIs were then transformed into triangular mesh models for visualization.

RNA extraction and sequencing

RNA extraction was performed using an RNA extraction kit (RNA isolater Total RNA Extraction Reagent R401-01; Vazyme, Nanjing, China). For small samples, such as ladybirds, we ground them using a homogenizer within lysate, transferred to an Eppendorf tube, and added to 1 mL of lysate.[52] Large body size samples, such as *L. migratoria*, were ground using a mortar and pestle, and 20 mg of the samples were transferred to 1 mL of lysate. At each time point, three biological replicates were collected, and each replicate included 10 individuals. RNA-seq was carried out using a TruePrep RNA Library Prep Kit for Illumina (TR501; Vazyme, Nanjing, China) and sequenced on a HiSeq 2500 platform. The original libraries were 150 bp paired-end and sequenced to 6 Gib. The information of RNA-seq raw data can be obtained from Tables S1–S3.

RNA-seq data processing

Firstly, we conducted a quality assessment of the raw data using FastQC (v0.11.4).[51] Following that, we removed low-quality sequences and adaptors from the raw data using TrimGalore (v0.6.7).[42] Reads from each library were mapped against the species reference genome using Hisat2 (v2.2.1).[45] Reference genomes were downloaded from InsectBase 2.0.[53] Alignment files were manipulated using samtools (v1.15.1).[46] Read counts for protein-coding genes were generated using featureCounts (v2.0.0).[47] DESeq2 (v1.42.0)[54] was used to generate the

differentially expressed genes and variance-stabilised counts for clustering analysis. We utilized the online version of eggNOG-mapper[48] to annotate the protein sequences. Following that, we extracted the GO terms and performed GO enrichment analysis for each species using the R package clusterProfiler.[35] We identified Single-Copy Orthologs (SC-OGs) and SNAP-Orthologs (SNAP-OGs) using Orthofinder (v2.5.4)[49] and OrthoSNAP (v0.0.1).[50] The protein sequences were obtained from GFF annotation files. The variance-stabilised counts of SC-OGs and SNAP-OGs were obtained using the standardize function with the *Z* SCORE algorithm from the R package Mfuzz (v2.62.0).[38] We employed two dimensionality reduction methods: Principal Component Analysis (PCA) and Uniform Manifold Approximation and Projection (UMAP).[23,24] K-means and Hierarchical clustering with "average" method[41,55] were also applied to cluster the gene expression patterns. Raw data of *D. melanogaster* developmental RNA-seqs were collected from previous studies.[21]

Time-specificity index

The time-specificity indexes are based on the Tau metric of tissue specificity.[25] Both indexes range from 0 to 1. A higher Tau value indicates a gene with more tissue-specific expression, while a lower Tau value suggests a more ubiquitously expressed gene. Genes exhibiting a Tau value greater than or equal to 0.85 are considered to demonstrate temporal-specific expression patterns. The Tau indexes are provided in Data S4. The *p*-values of two-sided Wilcoxon rank-sum test are provided in Table S8.

Gene expression patterns

For each species, we identified the expression patterns of 1:1 orthologs using c-means approach from the R package Mfuzz (v2.62.0).[38] The number of clusters was set to 8. Following that, we split the clusters into two main patterns: the first one where genes are highly expressed only during the larval stages (Early), and the second one where genes are highly expressed only during the prepupal or pupal stage (Late). The expression pattern of each orthologs is provided in Data S4.

Selective pressure

The coding sequences (CDS), with same expression pattern (early or late), were utilized for calculating the ratio of non-synonymous to synonymous substitution rates (Ka/Ks), whereas the upstream 2000 nt non-coding regions were employed for estimating the ratio of non-coding nucleotide substitution to neutral substitution rate (Kn/Ks). The sequences were aligned with MACSE.[43] KaKs_Caculator 3.0[44] were selected for Ka/Ks, Kn/Ks calculation. Orthologs from L. *migratoria* served as the reference. The results of KaKs_Caculator are available in Data S5–S16. The *p*-values of two-sided Wilcoxon rank-sum test are provided in Tables S9 and S10.

QUANTIFICATION AND STATISTICAL ANALYSIS

All Statistical analysis and plotting in this work were performed using R Software 4.0.4. The data are represented as mean ± SEM. Comparisons of wing volumes across different developmental stages were conducted using two-tailed Student's t-tests, with statistical significance defined as $p < 0.05$. Interspecific comparisons of Kn/Ks and Ka/Ks ratios were performed using the Wilcoxon rank-sum test. This non-parametric test was chosen to account for potential non-normal distributions in the evolutionary rate ratios across species. The test was conducted with a significance level set at $p < 0.05$.